Ballistic near-field heat transport in dense many-body systems

Ivan Latella,[1] Svend-Age Biehs,[2] Riccardo Messina,[3,4] Alejandro W. Rodriguez,[4] and Philippe Ben-Abdallah[1,5,*]

[1] *Laboratoire Charles Fabry, UMR 8501, Institut d'Optique, CNRS, Université Paris-Saclay, 2 Avenue Augustin Fresnel, 91127 Palaiseau Cedex, France*
[2] *Institut für Physik, Carl von Ossietzky Universität, D-26111 Oldenburg, Germany*
[3] *Laboratoire Charles Coulomb (L2C), UMR 5221 CNRS-Université de Montpellier, F- 34095 Montpellier, France*
[4] *Department of Electrical Engineering, Princeton University, Princeton, NJ 08544, USA*
[5] *Université de Sherbrooke, Department of Mechanical Engineering, Sherbrooke, PQ J1K 2R1, Canada.*

Radiative heat-transport mediated by near-field interactions is known to be superdiffusive in dilute, many-body systems. In this Letter we use a generalized Landauer theory of radiative heat transfer in many-body planar systems to demonstrate a nonmonotonic transition from superdiffusive to ballistic transport in dense systems. We show that such a transition is associated to a change of the polarization of dominant modes, leading to dramatically different thermal relaxation dynamics spanning over three orders of magnitude. This result could have important consequences on thermal management at nanoscale of many-body systems.

The theory of near-field radiative heat transfer has for many decades remained largely limited to two-body systems [1–6]. Recently, heat transport in many-body systems has also been considered in the context of nanoparticles [7–10] and multilayer geometries, such as photonic crystals [11, 12] and hyperbolic metamaterials [13–15]. The focus of much of this work has been the study of systems in which the steady-state temperature distribution of a set of internal bodies is a priori known and dictated via contact with large heat reservoirs. There are, however, situations in which a full study of heat transport necessitates an account of thermal relaxation through radiative channels. A first step in this direction has been made by generalizing Rytov's theory of fluctutational electrodynamics to describe radiative transfer in many-body geometries with varying temperature distributions, including nanoparticle systems [17–19], multilayer configurations [16, 20–28], and more generally, arbitrary geometries that include the possibility of inhomogeneously varying temperature profiles [29, 30]. Furthermore, heat transport within a collection of nanoparticles has been studied in Ref. [31], and the existence of a superdiffusive regime has been found, albeit within a dipolar approximation.

In the present Letter, we employ a recently developed, exact theoretical framework [32] to investigate near-field radiative heat transport in N-body systems consisting of parallel planar slabs separated by vacuum, in which radiation is the only source of thermal relaxation. We show that the temperature dynamics and steady-state profile of the system depend strongly on geometric parameters such as the system density, which imply different heat-transport regimes. In particular, we prove the existence of a nonmonotonic transition between a superdiffusive regime, previously observed in Ref. [31], and a ballistic regime that appears in denser media and that also leads to dramatically faster relaxation dynamics. We also show that this transition is associated with a change in the polarization of the dominant modes in the transport. In contrast to heat exchange in two-body geometries, where near-field heat transfer is dominated by transverse-magnetic (TM) modes, we found that transport in dense, many-body systems can have a significant contribution from transverse-electric (TE) modes.

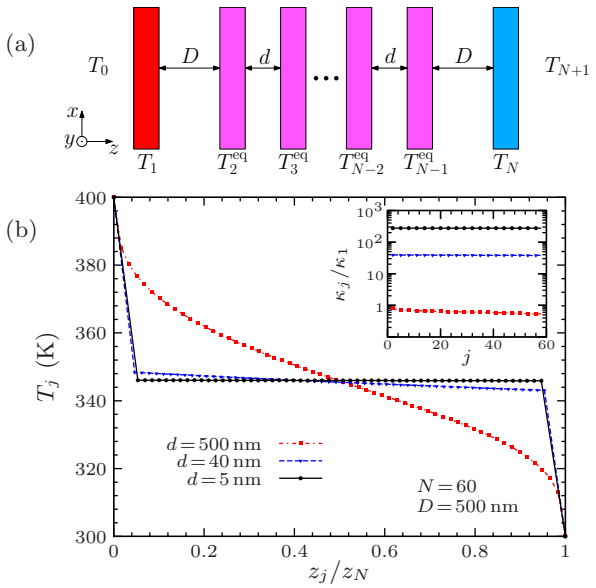

FIG. 1. (a) Schematic of an N-body system comprising $N-2$ planar slabs (purple) interacting with one another and with two external slabs at fixed temperatures T_1 (red) and T_N (blue). All internal separation distances d are identical while the coupling to the external thermostats depends on the separation distance D. In the steady state, each internal slab reaches a local equilibrium temperature $T_j^{\rm eq}$. (b) Steady-state temperature profile as a function of the normalized position z_j/z_N for a system of $N = 60$ SiC slabs of thickness 200 nm, for different d and fixed $D = 500$ nm. The inset shows the ratio of the effective internal conductivities κ_j/κ_1 (see text).

To begin with, let us consider a system composed of N planar slabs separated by vacuum, orthogonal to the z axis and assumed to be infinite in the x and y directions,

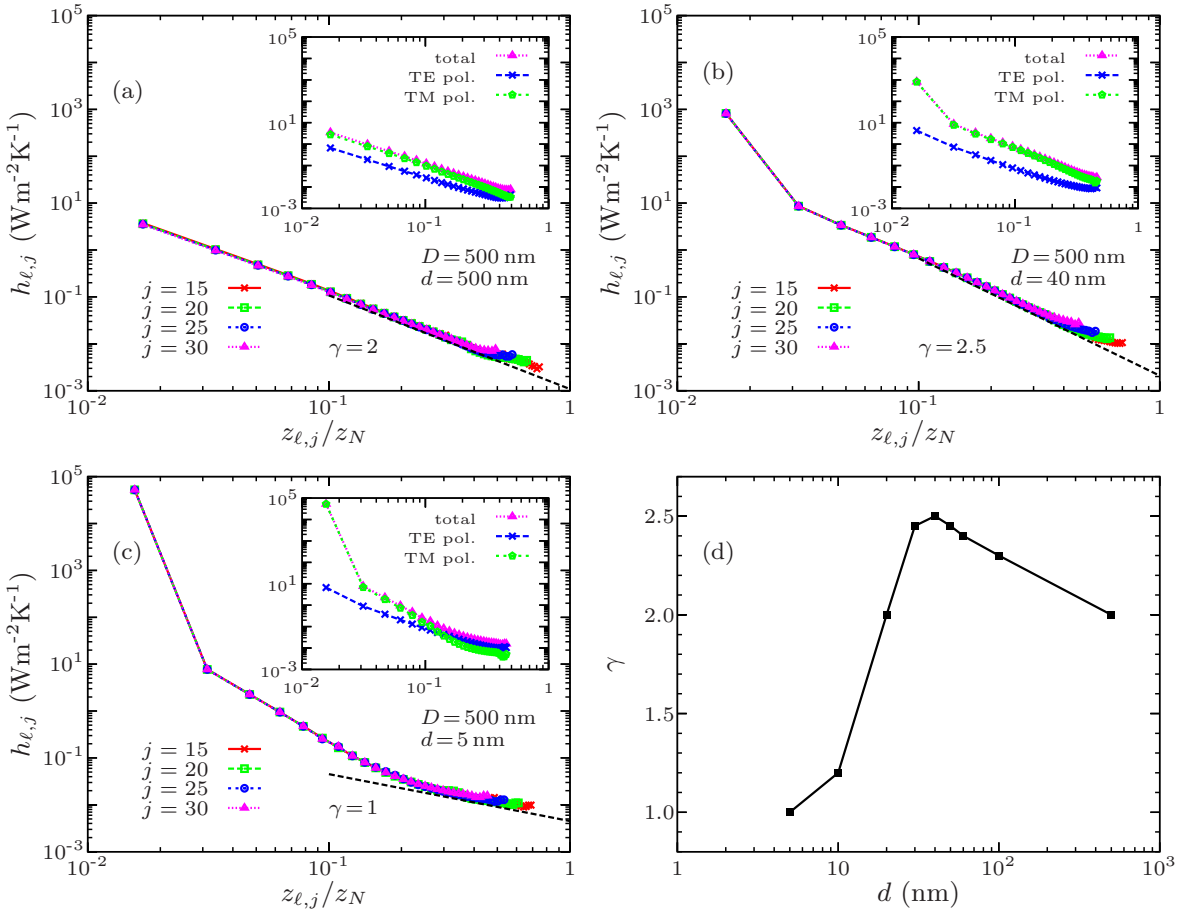

FIG. 2. Heat-transfer coefficients $h_{\ell,j}$ (see text) with respect to the normalized separation $z_{\ell,j}/z_N$, for fixed values of j and $D = 500\,\text{nm}$, and three values of (a) $d = 500\,\text{nm}$, (b) $d = 40\,\text{nm}$ and (c) $d = 5\,\text{nm}$. Dashed lines indicate the asymptotic behavior of $h_{\ell,j} \sim 1/z_{\ell,j}^{\gamma}$ at large separations. The value of γ indicates the nature of the heat-transport regime, from superdiffusive ($1 < \gamma < 3$) to ballistic ($\gamma \to 1$). The insets decompose $h_{\ell,j}$ for $j = 30$ into TE and TM polarization contributions. (d) Exponent γ as a function of d.

as sketched in Fig. 1(a). The thicknesses δ_j of the bodies are assumed to be equal, $\delta_j = \delta$ for $j = 1, \ldots, N$, and below we take $\delta = 200\,\text{nm}$. The temperatures of slabs 1 and N, referred to as *external* slabs, are held constant at $T_1 = 400\,\text{K}$ and $T_N = 300\,\text{K}$, respectively, via contact with an external reservoir, while all the other *internal* slabs are allowed to reach their own equilibrium temperature T_j^{eq} ($j = 2, ..., N-1$). We also consider that the system is immersed in an environment (thermal bath) at temperature $T_0 = T_{N+1} = T_B = 300\,\text{K}$. Below D denotes the distance between slabs 1 and 2, as well as slabs $N-1$ and N, whereas d is the distance between adjacent, internal slabs. Furthermore, in our numerical simulations we assume that all the bodies are made of silicon carbide (SiC), whose permittivity at frequency ω can be described by the Drude-Lorentz model [33] $\varepsilon(\omega) = \varepsilon_\infty \frac{\omega_L^2 - \omega^2 - i\Gamma\omega}{\omega_T^2 - \omega^2 - i\Gamma\omega}$, where $\varepsilon_\infty = 6.7$ is the high frequency dielectric constant, $\omega_L = 1.83 \times 10^{14}\,\text{rad/s}$ is the longitudinal optical phonon frequency, $\omega_T = 1.49 \times 10^{14}\,\text{rad/s}$ is the transverse optical phonon frequency, and $\Gamma = 8.97 \times 10^{11}\,\text{rad/s}$ is the damping rate. As shown in Ref. [32], the net radiative flux per unit surface received by any given slab j can be written as a sum over the energy exchanged with every other body $\varphi_{\ell,j}$, with

$$\varphi_j = \sum_{\ell \neq j} \varphi_{\ell,j} = \sum_{\ell \neq j} \int_0^\infty \frac{d\omega}{2\pi} \int_0^\infty \frac{dk}{2\pi} k \sum_p \hbar\omega\, n_{\ell,j} \mathcal{T}^{\ell,j}, \quad (1)$$

where $\ell \neq j$ runs from 0 to $N+1$ (including the external environment). In this expression $p = \text{TE}, \text{TM}$ denotes the two polarizations, k is the parallel component of the wave vector, and $n_{\ell,j} \equiv n_\ell - n_j$, with $n_j = \left(e^{\hbar\omega/k_B T_j} - 1\right)^{-1}$ denoting the Bose distribution. The Landauer coefficient $\mathcal{T}^{\ell,j} = \mathcal{T}^{\ell,j}(\omega, k, p)$, which can vary between 0 and 1, describes the contribution of each mode (ω, k, p) to the energy exchange and depends on the geometrical and material properties of the slabs [32]. The local equilibrium temperatures T_j^{eq} of the internal slabs can be calculated by requiring that in the steady state,

the net flux received by each slab is zero, that is by solving the system of transcendental equations, $\varphi_j = 0$ for $j = 2, \ldots, N-1$. The steady-state temperature profiles inside the system are shown in Fig. 1(b) for $N = 60$ slabs and for several separation distances $d \in \{5, 40, 500\}$ nm and fixed $D = 500$ nm. We first observe that, while for $d = D = 500$ nm the temperature profile decays smoothly, the configurations having a smaller d reveal a more dramatic jump between the external and the adjacent (T_2, T_{N-1}) temperatures, in which case the internal slabs become much more thermally isolated from the reservoirs. Moreover, the shape of the profile clearly depends on d, becoming nonlinear for $d = 500$ nm, close to linear for $d = 40$ nm, and nearly constant for $d = 5$ nm.

We now describe how the main features characterizing heat transport in this geometry, i.e. the temperature profile near the boundary and within the bulk, depend on both D and d. As far as the former is concerned, the main parameter of interest is the relative coupling strength of boundary versus internal slabs, quantified by defining an effective, thermal conductivity $\kappa_j = \varphi_{j,j+1} d_j/(T_j - T_{j+1})$, where $d_1 = d_{N-1} = D$ and $d_j = d$ for $j = 2, \ldots, N-2$. The ratio κ_j/κ_1, which can be interpreted as a measure of the boundary thermal resistance, is plotted in the inset of Fig. 1(b), showing that κ_j is almost constant within the chain of internal slabs and that κ_j/κ_1 is close to unity for $d = 500$ nm, increases with decreasing d, and reaches two orders of magnitude when $d = 5$ nm. As illustrated in Fig. 3 below, the smoothness of the temperature profile near the boundary only depends on the ratio d/D. We next focus on the shape of the temperature profile within the bulk, which is closely related to the transport regime and requires a more nuanced description of the problem.

As show in Ref. [31], to understand and classify the various transport regimes in this kind of system, it is useful to study the power exchanged between layers in the limit of large N. For convenience, we make the simplifying assumption that the temperature differences involved in the system are small enough to allow a linearization of $n_{\ell,j}$. Under this assumption, the net flux on slab j reads,

$$\varphi_j \simeq \sum_{\ell \neq j} h_{\ell,j}(T_\ell - T_j), \tag{2}$$

where we have introduced the heat-transfer coefficients,

$$h_{\ell,j} = \int_0^\infty \frac{d\omega}{2\pi} \int_0^\infty \frac{dk}{2\pi} k \sum_p \hbar\omega \frac{\partial n_j}{\partial T_j} \mathcal{T}^{\ell,j}. \tag{3}$$

Assuming that $h_{\ell,j} \sim 1/z_{\ell,j}^\gamma$, for some exponent $\gamma = 1+\alpha$, where $z_{\ell,j} \equiv |z_\ell - z_j|$ and z_j denotes the position of the j-th layer, one finds that in the continuum limit of $N \to \infty$ (with fixed Nd), $T_j \to T(z)$ and

$$\varphi_j \to \varphi(z) \sim (-\Delta)^{\alpha/2} T(z), \tag{4}$$

where $(-\Delta)^{\alpha/2}$ is the fractional Laplacian defined in 1D

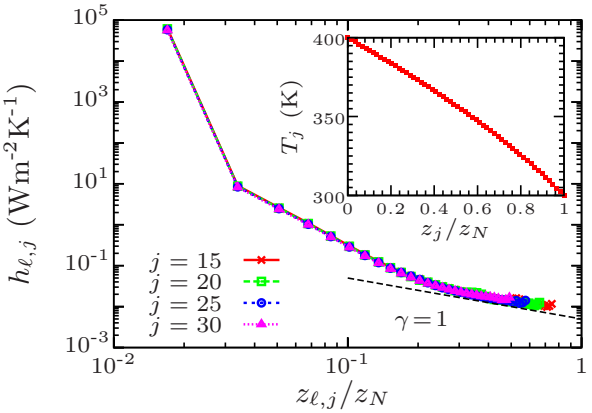

FIG. 3. Heat-transfer coefficients $h_{\ell,j}$ as a function of the normalized separation $z_{\ell,j}/z_N$, for $D = d = 5$ nm, along with the corresponding steady-state temperature profile (inset).

systems as $(0 < \alpha < 2)$

$$(-\Delta)^{\alpha/2} T(z) = c_\alpha \, \mathrm{PV} \int_{-\infty}^{\infty} \frac{T(z) - T(z')}{|z - z'|^{1+\alpha}} dz', \tag{5}$$

with c_α a constant [34, 35] and where PV denotes the principal value. As we discuss below, Eq. (5) can be used as a tool to relate the asymptotic, large-distance behavior of $h_{\ell,j}$ to the regime of heat transport. It follows from Eq. (5) that the regime of heat transport is superdiffusive when $1 < \gamma < 3$. In the limiting case $\gamma \to 3$, the fractional Laplacian degenerates into its classical form and the regime of transport is diffusive. On the other hand, as $\gamma \to 1$, the fractional Laplacian approaches the identity operator and the transport becomes ballistic.

Figure 2 shows $h_{\ell,j}$ for multiple values of j as a function of ℓ, for the same system of Fig. 1. When $d = 500$ nm, corresponding to a SiC volume fraction of 28.5% (dilute system), $h_{\ell,j}$ asymptotically decays as $1/z_{\ell,j}^2$, showing that indeed the heat transport is superdiffusive, as in simple dipolar systems [31]. Note that the small variations in $h_{\ell,j}$ at the extreme end of the curves come from finite-size effects and are therefore not taken into account in the scaling analysis. When $d = 100$ nm [see Fig. 2(b)], the exponent in the scaling of $h_{\ell,j}$ increases, but the transport regime remains superdiffusive. On the other hand, when $d = 5$ nm, corresponding to a SiC volume fraction of 97.5% (dense system), $h_{\ell,j} \sim 1/z_{\ell,j}$, in which case the transport is ballistic and the system experiences an effectively weak thermal resistance within the bulk. Figure 2(d) shows γ as a function of d, illustrating a nonmonotonic behavior as the system transitions from a superdiffusive to a ballistic regime. Furthermore, as illustrated on the insets of Fig. 2, which show the contributions of TE and TM modes to $h_{\ell,j}$, we find that TE modes dominate and hence determine the (ballistic) transport regime at small d; in contrast, TM modes are the main heat carriers in the superdiffusive regime, which

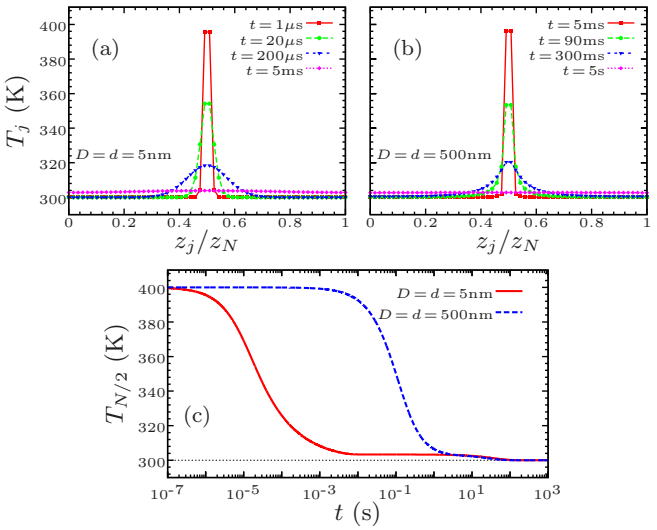

FIG. 4. Temporal evolution of the temperature profile for a system ($N = 60$) interacting with a thermal bath at $T_B = T_0 = T_{N+1} = 300\,\mathrm{K}$. At $t = 0$, all bodies have temperature T_B except the two central slabs, which have $T_{N/2} = T_{N/2+1} = 400\,\mathrm{K}$. (a) Ballistic regime ($D = d = 5\,\mathrm{nm}$). (b) Superdiffusive regime ($D = d = 500\,\mathrm{nm}$). (c) Temperature of slab $N/2$ as a function of time in the two previous cases.

is the case in typical two-body geometries involving polaritonic resonances. This surprising result is a clear indication of the complexities and richness of heat transport in many-body systems.

Figure 3 shows $h_{\ell,j}$ along with the temperature profile (inset) for $d = D = 5\,\mathrm{nm}$. Comparing the former to the results in Fig. 2(c), one confirms that the transport regime is independent of D and therefore only depends on the density within the bulk, determined by d. On the other hand, comparing the temperature profile in Fig. 3 to those in Fig. 1, one infers that indeed only the ratio d/D (or thermal resistance) controls the smoothness of the profile near the boundaries.

Finally, we investigate the impact of the previously considered transport regimes on the relaxation dynamics of the system. Given an initial temperature distribution $\boldsymbol{T}(0) = \big(T_1(0), ..., T_N(0)\big)$, the temperatures of the bodies $\boldsymbol{T}(t) = \big(T_1(t), \ldots, T_N(t)\big)$ at any give time $t > 0$ are solutions of the energy balance equation,

$$\partial_t \boldsymbol{T} = \mathbb{K} \cdot \boldsymbol{T} + \boldsymbol{S}, \tag{6}$$

where $\mathbb{K} = \mathbb{H}/(C\delta)$ is a stiffness matrix defined in terms of the heat-transfer matrix $\mathbb{H}$, with elements $[\mathbb{H}]_{\ell,j} = h_{\ell,j}$ ($\ell, j = 1, \ldots, N$), and the SiC heat capacity per unit volume [36] $C = 8.15\,\mathrm{J{\cdot}cm^{-3}{\cdot}K^{-1}}$. Here, $h_{j,j} = -\sum_{\ell \neq j} h_{\ell,j}$ quantifies the emission rate of body j in the presence of the other slabs, while $\boldsymbol{S} = \frac{T_B}{C\delta}(h_{0,1} + h_{N+1,1}, \ldots, h_{0,N} + h_{N+1,N})$ denotes the source term corresponding to power supplied by the bath to each layer. Equation (6) is simply a discrete form of the fractional diffusion equation, the fractional exponent being related to the scaling of $h_{\ell,j}$, whose solution in the steady state reads $\boldsymbol{T}^{\mathrm{eq}} = -\mathbb{K}^{-1} \cdot \boldsymbol{S} = (T_B, \ldots, T_B)$. Since $h_{\ell,j}$ depends weakly on T_j, we assume that $\mathbb{K}$ is a time-independent matrix, in which case the time evolution of the temperature profile is thus given by $\boldsymbol{T}(t) = \exp(\mathbb{K}t) \cdot [\boldsymbol{T}(0) - \boldsymbol{T}^{\mathrm{eq}}] + \boldsymbol{T}^{\mathrm{eq}}$. Figure 4 shows the temporal evolution of the system in both superdiffusive and ballistic regimes, assuming an initial temperature profile corresponding to heating of the two central slabs to a temperature of 400 K. We observe a strong increase of the relaxation dynamics in the ballistic regime compared to the superdiffusive case, showing a difference in characteristic equilibration scales of nearly three orders of magnitude (from microseconds to milliseconds for a reduction of about half the initial overheating). We also observe that, as previously observed in dilute media [17], the relaxation process occurs in two distinct timescales. First, all layers thermalize at the same temperature through near-field interactions in about 5 ms in dense media (seconds in the diluted case). Subsquently, all layers collectively cool down to the ambient temperature through far-field interactions with the thermal bath.

In conclusion, we have studied a many-body geometry of planar slabs which exhibits a transition in the regime of radiative heat-transport, from ballistic to superdiffusive, with respect to slab density. Our predictions reveal complex, many-body effects in addition to dramatically different relaxation dynamics, depending on the transport regime. These effects could have important implications for thermal management at nanoscale in devices involving multiple, interacting elements thermally coupled in the near field.

Acknowledgments—We acknowledge the use of the computing center MésoLUM of the LUMAT research federation (FR LUMAT 2764). This work was partially supported by the National Science Foundation under Grant no. DMR-1454836 and by the Princeton Center for Complex Materials, a MRSEC supported by NSF Grant DMR-1420541.

* pba@institutoptique.fr

[1] D. Polder and M. van Hove, Phys. Rev. B **4**, 3303 (1971).
[2] J. J. Loomis and H. J. Maris, Phys. Rev. B **50**, 18517 (1994).
[3] K. Joulain, J.-P. Mulet, F. Marquier, R. Carminati, and J.-J. Greffet, Surf. Sci. Rep. **57**, 59 (2005).
[4] A. I. Volokitin and B. N. J. Persson, Rev. Mod. Phys. **79**, 1291 (2007).
[5] C. R. Otey, L. Zhu, S. Sandhu, and S. Fan, J. Quant. Spec. Rad. Trans. **132**, 3 (2014).
[6] B. Song, A. Fiorino, E. Meyhofer, and P. Reddy. AIP Advances **5**, 053503 (2015).
[7] P. Ben-Abdallah, Appl. Phys. Lett. **89**, 113117 (2006).
[8] P. Ben-Abdallah, K. Joulain, J. Drevillon and C. Le Goff, Phys. Rev. B **77**, 075417 (2008).

[9] P. Ben-Abdallah, S.-A. Biehs, and K. Joulain, Phys. Rev. Lett. **107**, 114301 (2011).

[10] J. Ordonez-Miranda, L. Tranchant, K.Joulain, Y. Ezzahri, J. Drevillon, and S. Volz, Phys. Rev. B **93**, 035428 (2016).

[11] W. T. Lau, J.-T. Shen, G. Veronis, S. Fan, and P. V. Braun, Appl. Phys. Lett. **92**, 103106 (2008).

[12] W. T. Lau, J.-T. Shen, and S. Fan, Phys. Rev. B **80**, 155135 (2009).

[13] J. Liu and E. Narimanov, Phys. Rev. B **91**, 041403(R) (2015).

[14] S.-A. Biehs, S. Lang, A. Yu. Petrov, M. Eich, and P. Ben-Abdallah, Phys. Rev. Lett. **115**, 174301 (2015).

[15] R. Messina, P. Ben-Abdallah, B. Guizal, M. Antezza and S.-A. Biehs, Phys. Rev. B **94**, 104301 (2016).

[16] R. Messina, M. Antezza, and P. Ben-Abdallah, Phys. Rev. Lett. **109**, 244302 (2012).

[17] R. Messina, M. Tschikin, S.-A. Biehs, and P. Ben-Abdallah, Phys. Rev. B **88**, 104307 (2013).

[18] V. Yannopapas and N. V. Vitanov, Phys. Rev. Lett. **110**, 044302 (2013).

[19] M. Nikbakht, EPL **110**, 14004 (2015).

[20] V. Kubytskyi, S.-A. Biehs, and P. Ben-Abdallah, Phys. Rev. Lett. **113**, 074301 (2014).

[21] R. Messina and M. Antezza, Phys. Rev. A **89**, 052104 (2014).

[22] P. Ben-Abdallah and S. A. Biehs, Phys. Rev. Lett. **112**, 044301 (2014)

[23] S. A. Dyakov, J. Dai, M. Yan, and M. Qiu, J. Phys. D: Appl. Phys. **48**, 305104 (2015)..

[24] I. Latella, A. Pérez-Madrid, J. M. Rubi, S.-A. Biehs, and P. Ben-Abdallah, Phys. Rev. Applied **4**, 011001 (2015).

[25] P. Ben-Abdallah, Phys. Rev. Lett. **116**, 084301 (2016).

[26] B. Müller, R. Incardone, M. Antezza, T. Emig, and M. Krüger, Phys. Rev. B **95**, 085413 (2017).

[27] R. Messina, W. Jin and A. W. Rodriguez, Phys. Rev. B **94**, 205438 (2016).

[28] R. Messina, W. Jin and A. W. Rodriguez, Phys. Rev. B **94**, 121410(R) (2016).

[29] S. Edalatpour and M. Francoeur, Phys. Rev. B **94**, 045406 (2016).

[30] W. Jin, R. Messina, and A. W. Rodriguez, Phys. Rev. B **95**, 161409(R) (2017).

[31] P. Ben-Abdallah, R. Messina, S.-A. Biehs, M. Tschikin, K. Joulain, and C. Henkel, Phys. Rev. Lett. **111**, 174301 (2013).

[32] I. Latella, P. Ben-Abdallah, S.-A. Biehs, M. Antezza and R. Messina, Phys. Rev. B **95**, 205404 (2017).

[33] *Handbook of Optical Constants of Solids*, edited by E. Palik (Academic Press, New York, 1998).

[34] I. Podlubny, *Fractional Differential Equations* (Academic Press, London, 1999).

[35] S. G. Samko, A. A. Kilbas, and O. I. Maritchev, *Fractional Integrals and Derivatives* (Gordon and Breach, New York, 1993).

[36] A. Sommers, Q. Wang, X. Han, C. T'Joen, Y. Park, and A. Jacobi, Appl. Therm. Eng. **30**, 1277 (2010).